The Use of Sectional Imaging with CT and MRI for Image-Guided Therapy

2

Johannes C. Athanasios Dimopoulos and Elena Fidarova

2.1 Introduction

Sectional imaging is integrated in each link of the modern radiotherapy chain, from diagnostic procedures to target volume definition to treatment planning, dose delivery, and verification. While CT is widely used for modern EBRT, including intensity modulated radiotherapy (IMRT) and image-guided radiotherapy (IGRT), MRI represents the gold standard for IGBT for gynecological malignancies (see Chap. 5, Sect. 5.4).

High-precision radiotherapy techniques offer the option of enhancement of the therapeutic ratio, because the dose to the target is escalated and the normal organs are spared. However, in order to increase conformity, accurate target and organ delineation performed according to standardized protocols is required. Additionally, inter-/intrafraction variation due to tumor shrinkage and changes in dimensions and topography of the normal organs has to be taken into account, thus representing the main challenge for successful application of IGRT.

To reduce contouring uncertainties and to identify inter-/intrafraction variation with high accuracy, a radiation oncologist has to apply image acquisition protocols adapted to the needs of image-guided therapy, to analyze sectional images with particular attention to tumor regression, regions of potential tumor spread, and lymph nodes regions. This chapter aims to cover important issues of CT and MRI application for image-guided therapy.

J.C.A. Dimopoulos (✉)
Director of Department of Radiation Therapy, Metropolitan Hospital,
9 Ethn. Makariou and El. Venizelou, 18547 Athens, Greece
e-mail: adimopoulos@metropolitan-hospital.gr

E. Fidarova
Department of Radiotherapy, Vienna General Hospital, Medical University of Vienna,
Währinger Gürtel 18-20, 1090 Vienna, Austria
e-mail: Elena.fidarova@akhwien.at

A.N. Viswanathan et al. (eds.), *Gynecologic Radiation Therapy*,
DOI: 10.1007/978-3-540-68958-4_2, © Springer-Verlag Berlin Heidelberg 2011

2.2 General Technical Issues Regarding the Use of Sectional Imaging for Image-Guided Therapy

CT is the standard imaging modality for 3D conformal EBRT and IMRT of the pelvis. It provides information about the electron density of tissues that is required for the dose calculation algorithms of all the commercially available treatment planning systems. CT also lacks peripheral image distortion that is characteristic of MRI. Modern CT scanners obtain 64 slices for each turn of the gantry and offer the possibility of image acquisition of the entire abdomen and pelvis in less than 1 min. For in-room imaging, both multi-slice CT and cone-beam CT (CBCT) can be used. The new generation of accelerators is equipped with CBCT mounted on the gantry. This technical solution allows detecting individual variations under treatment conditions and their on-line correction [1, 2]. The use of such volumetric image-guidance has increased the demand for adaptive replanning [1].

MRI enables improved soft tissue depiction and gives detailed information about pelvic topography and tumor regression during radiotherapy [3–5]. It has to be noted though, that MRI is not routinely implemented for EBRT treatment planning mainly due to two major limitations: intrinsic spatial image distortion and missing electron density information [6, 7]. This implies that if MRI scans are used for treatment planning, tissue attenuation coefficients have to be assigned manually or a homogeneous attenuation has to be assumed within all image regions [6, 7]. An alternate option is co-registration and fusion of MR and CT images, which allow achieving desirable imaging information and creating optimal conditions for precise dose calculation [8, 9]. The problem of MR image distortions can be resolved by applying different image correction methods [10–13].

Low-field 0.2–0.5 T (Tesla) open MRI scanners offer improved patient accessibility and are suitable for claustrophobic patients [4]. However, the image quality of low-field scanners is not equivalent to the image quality of those with standard magnetic field strength of 1.5 T and higher. Therefore, scanners with 3 T are increasingly utilized in the radiology community. With higher field strength, the signal-to-noise ratio is increasing and the voxel volume can be reduced [14]. Image distortion is also increasing with increasing field strength [7]. Higher magnetic fields, like 7 and 8 T have been installed only in a few research centers as they present some technical challenges, e.g., the safety limits can be exceeded due to higher gradient amplitudes and radiofrequency power deposition [14]. Furthermore, they do not automatically produce better diagnostic images because of dielectric resonance effects [15].

2.3 Key Issues of Image Acquisition

Pelvic CT used for EBRT should be performed after administration of intravenous contrast agents. Additional improvement can be achieved by the use of oral iodine or barium-based contrast material. In the case of IGBT, intravenous contrast also assists in the identification of the superior border of the cervix due to visualization of the uterine vessels [16].

Retrograde application of bladder and rectal contrast before CT scanning improves delineation of these structures [16].

MR image acquisition protocols also need to be adapted to the needs of IGRT and IGBT. T2-weighted MRI sequences are considered the gold standard for IGRT and IGBT for gynecological malignancies [3, 4]. Vaginal contrast, e.g., with ultrasound gel, used for diagnostic scans improve visualization of the vaginal walls and lower parts of the cervix [4]. Bowel motion can be reduced by intravenous (e.g., *N*-Butylscopolan) or intramuscular (e.g., Glucagon chlorhydrate) drug administration. Use of MRI-compatible applicators and probes, vaginal packing impregnated with contrast agents (e.g., gadolinium, dilution 1:10) and a Foley catheter filled with contrast media (e.g., gadolinium, dilution 1:1) leads to clear visualization of relevant structures [4]. Only limited data about the impact of MR image orientation on contouring for IGBT is available [17]. However, current recommendations suggest using images orientated parallel and orthogonal to the applicator (sources) axes to obtain a "brachytherapy orientated view" (BOV) [18].

2.4 Issues of CT/MR Image Characteristics

CT scans provide information about topographic changes caused by tumor shrinkage, organ motion, and insertion of the brachytherapy applicator [19–21]. The normal organ contours (sigmoid colon, rectum, urinary bladder, vagina) as well as borders between organs and uterine parts (corpus, cervix) are often not clearly visible on native CT scans [22]. Improved visualization of these contours can be achieved by the use of contrast media, but even in this case organ walls are not clearly visualized [21]. Finally, the spatial relationship between the brachytherapy applicator, uterus (cervix, corpus), and surrounding organs becomes visible on CT images [4, 18, 21, 22].

However, there are some inherent limitations of CT for 3D delineation of relevant structures for IGRT and IGBT. The uterus is displayed as a homogenous organ located in the center of the true pelvis. Distinction between different patho-anatomical parts (corpus, cervix, tumor mass(es)), relies on indirect information about the topography of the endometrial cavity and uterine artery [16, 21, 23]. Parametrial ligaments and uterine arteries can be identified on CT with a wide variation of shapes and thicknesses [16, 21, 23]. Accurate detection of tumor and parametrial infiltration on CT is challenging compared to MRI [21, 24, 25]. CT provides limited information about radiation changes and distinction between cervix and residual disease (within the parametria and the uterus) [16, 21].

MRI appears to discriminate soft tissue and tumor in the pelvis and has the capability of imaging in multiple planes, as compared to CT [26]. A comparison between MR and CT as imaging modalities used for IGBT, revealed no significant differences in volume sizes and DVH parameters for the organs at risk (OAR), but for target volumes, CT-based contouring significantly overestimated the contour width when compared to MRI (Fig. 2.1) [16].

Information essential to improve IGRT and IGBT, like tumor extent, topography, and regression, as well as topography of patho-anatomical structures, is provided by MRI

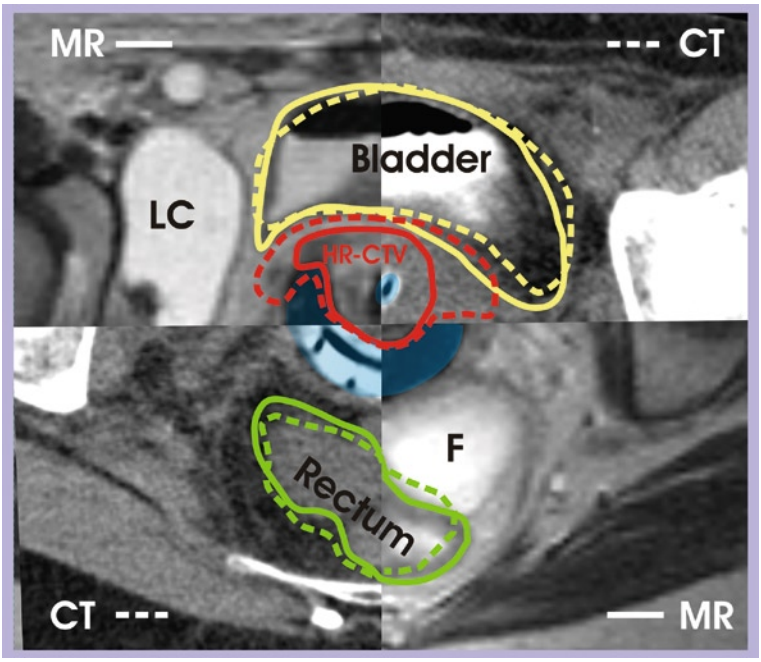

Fig. 2.1 Image fusion between axial computed tomography (CT) and magnetic resonance (MR) scans at time of brachytherapy. Bladder, rectum, and High Risk (HR) Clinical Target Volume (CTV) are contoured (CT – *dotted line*, MR – *solid line*). Organs at risk (OAR) contours deviate only slightly, whereas HR CTV is larger on CT, especially in lateral directions. Blue transparent color indicates tandem-ring applicator, which is depicted as a homogeneous black structure in magnetic resonance imaging (MRI). On the contrary, details of the applicator (source channel, holes for needles) are clearly visible on a CT scan (LC, lymphocyst after laparoscopic lymph node staging; F, free fluid in the pouch of Douglas)

[3, 4, 27–29]. A systematic analysis of MRI findings before EBRT and at the time of brachytherapy with the applicator in place, provided information helpful to reduce uncertainties regarding the definition of gross target volume (GTV), clinical target volume (CTV), and patho-anatomical structures (Fig. 2.2) [4]. Finally, it has been shown that the parametrial space, as the region of potential tumor spread, can be defined on axial MR images based on visible radiological criteria [4].

The most important image characteristics, as well as the pearls and pitfalls of CT and MRI for image-guided therapy are summarized in Table 2.1.

2.5 The Issue of Lymph-Node Delineation for High-Precision and Image-Guided EBRT

The detection of pathologic enlarged lymph nodes with sectional imaging is of major importance for IGRT. The precision of CT and MRI for the detection of lymph node

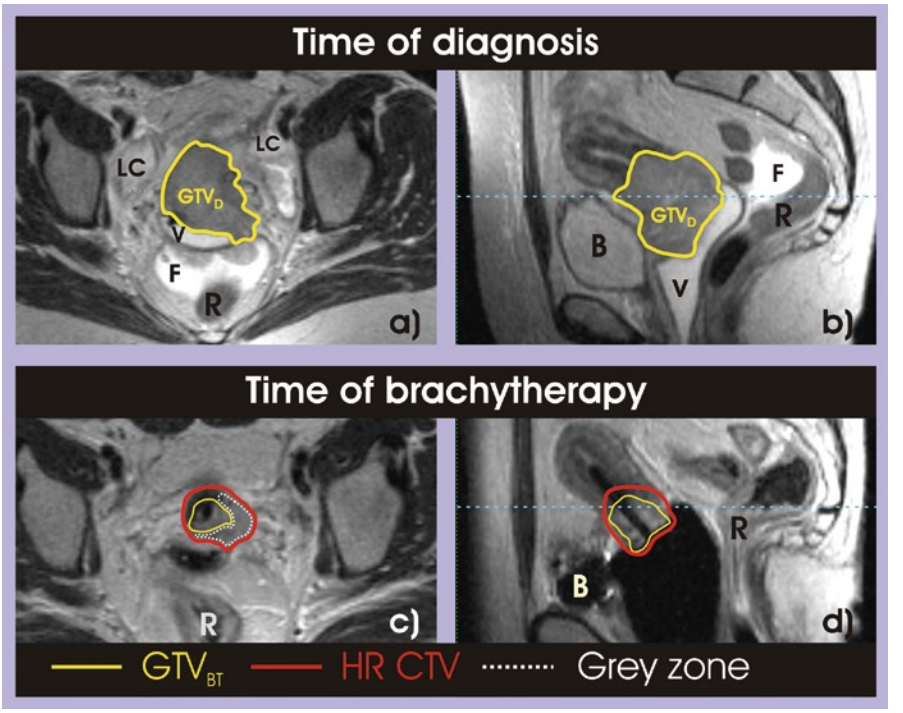

Fig. 2.2 MRI scans of a patient with FIGO IIB cervical cancer at time of diagnosis ((**a**) – axial plane, (**b**) – sagittal plane) and at time of brachytherapy ((**c**) – axial plane, (**d**) – sagittal plane). Tumor at time of diagnosis (GTV_D), which replaces the uterine cervix (**a**, **b**) and invades the left parametrium (**a**), is depicted as a homogeneous intermediate signal intensity mass. At the time of brachytherapy, HR CTV consists of high signal intensity residual tumor (GTV_{BT}), intermediate signal intensity "grey zones" and low signal intensity cervical tissue (**c**, **d**). *Dotted blue line* on sagittal images represents the level at which the correspondent axial scan was obtained (LC, lymphocyst after laparoscopic lymph node staging; F, free fluid in the pouch of Douglas; V, vagina contrasted with ultrasound gel; B, bladder; R, rectum)

metastasis is comparable [30–32]. Since both imaging modalities rely on size criteria (short axis >1 cm) for the detection of pathologic lymph nodes, the sensitivity of these methods is rather low, ranging between 40% and 70% [33–35]. Lymph node specific MRI contrast agents, e.g., ultrasmall particles of iron oxide (USPIO), show the potential of improving sensitivity for the prediction of lymph node metastasis. In the study of Rockall et al. the sensitivity increased from 29% using standard size criteria, to 93% using USPIO criteria based on a node-by-node approach, and from 27% to 100% based on a patient-by-patient approach [34]. FDG PET/CT is more accurate in identifying nodal metastases as the nodes do not need to be enlarged to be PET/CT positive. The reported sensitivity and specificity of PET/CT is within a range of 50–75% and 90–99% respectively [36–38].

Table 2.1 General characteristics with pearls and pitfalls of computed tomography (CT) and magnetic resonance (MR) for the different stages of image-guided therapy

	General characteristics					
	Soft tissue depiction	Image acquisition	Contrast media	Multiplanar imaging	Radiation exposure	Scanning time
MRI	Superior quality on T2-weighted sequences	Specific protocols required	Not obligatory needed	without reconstruction	No	Long
CT	I nferior quality	Specific protocols required	Recommended	only with reconstruction	Yes	Short
	Diagnostic scan					
	Tumor detection	Parametrial invasion	Invasion of organs	Invasion of vagina	LN status	Recurrence detection
MRI	Estimation of dimensions within 0.5 cm compared to pathology specimen. Detection of endocervical growth and uterine corpus invasion is possible	High accuracy for: –Distinction between stromal and parametrial invasion –Estimation of degree of parametrial invasion	High accuracy in prediction of infiltration of surrounding organs	High accuracy in predicting vaginal invasion, if vaginal contrast is used (e.g., ultrasound gel)	CT and MRI have similar inaccuracy in detecting LN metastases	Dynamic contrast-enhanced MRI enables differentiating tumor recurrence from radiation fibrosis
CT	Inaccurate estimation of tumor dimensions even with contrast enhancement and inability to detect uterine corpus invasion	Low accuracy in distinction between parametrial tumor spread and normal parametrial tissue	Early invasion of bladder and rectum is not reliably detectable	Low accuracy in predicting vaginal infiltration, especially at early stages	CT and MRI have similar accuracy in detecting LN metastases	CT is of low predictive value for differentiation between radiation fibrosis and recurrence

	IGRT scans (in addition to information gained from diagnostic scans)				
	Tumor regression			Organ changes	
MRI	Accurate quantitative estimation of tumor regression during the entire course of radiotherapy is possible. Distinction between macroscopic visible (residual) tumor mass(es), pathologic residual tissue including edema, inflammation, fibrosis and tumor cells ("grey zones"), and surrounding tissue possible			Reliable detection of changes in organ position and volume possible	
CT	Quantitative estimation of tumor regression not reliable. Distinction between macroscopic visible (residual) tumor mass(es), pathologic residual tissue ("grey zones"), and surrounding tissue not possible			Reliable detection of changes in organ position and size possible	
	Brachytherapy scans				
	Target definition	Parametrial invasion	Invasion of organs	Invasion of vagina	Applicator depiction
MRI	Different parts of HR CTV [GTV = macroscopic tumor mass(es), ("grey zones") and cervix] are detectable	Detection of macroscopic tumor and residual pathologic tissue within the parametria possible	Detection of residual organ involvement possible	Detection of residual vaginal involvement possible	Inferior quality on T2-weighted sequences
CT	Different parts of HR CTV are not detectable	Reliable detection of macroscopic tumor and residual pathologic tissue within the parametria not possible	Detection of residual organ involvement not always possible	Detection of residual organ involvement not always possible	Superior quality – Different parts of the applicator (e.g., source channel, wholes) are visible

Table 2.2 Location of assessed lymph nodes in relation to adjacent blood vessels

LN group		Average distance (range), mm[a]		
		Chao et al. [41]	Taylor et al. [43][b]	Diniwell et al. [42][c]
Common iliac	Right	12 (5–16)	–	–
	Left	16 (6–22)	–	–
	Ventral	0.3 (0–2)	–	–
	Not specified	–	7	7 (3–21)
External iliac	Medial	–	7	–
	Anterior	–	7	–
	Lateral	Right 16 (11–22)[d] Left 14 (7–17)[d]	15	–
	Not specified	–	–	7 (3–10)
Internal iliac		–	5	7 (3–14)
Obturator		–	3	8 (4–19)
Inguinal	Right	17 (7–28)	–	–
	Left	15 (8–23)	–	–
Para-aortic	Distal	–	–	9 (4–23)
	Ventral	2 (0–6)	–	–
	Right	9 (6–15)	–	–
	Left	22 (10–45)	–	–

[a]All distances were rounded
[b]At least 90% of LN covered by the given margin
[c]90% of LN was localized within given distance
[d]Relative to pelvic side wall

Some recent studies focused on the definition of guidelines for the delineation of the pelvic nodal target volume [39, 40]. Table 2.2 summarizes the margins proposed by different authors [41–43]. Chao and Lin suggested guidelines for IMRT of gynecological tumors based on lymphangiogram-assisted CT lymph-node delineation [41]. The authors recommend margins of 15–20 mm, with some modifications. Diniwell and colleagues used MRI scans with the contrast agent ferumoxtran-10 to investigate the nodal pelvic CTV [42]. In their study a 3D margin of 9–12 mm around the blood vessels and a margin of 22 mm medial to the pelvic sidewall were required to cover 90% of nodal tissue in 90% of patients [42]. Taylor et al. used MRI with iron oxide particles as a contrast agent and generated five CTVs with modified margins of 3–15 mm around the iliac vessels [43]. Appropriate lymph node coverage was achieved when a modified margin of 7 mm was used. Vilarino-Varela et al. confirmed these results [44].

The margins proposed by the recent RTOG consensus guidelines for delineation of the CTV for postoperative pelvic IMRT are mainly in agreement with the findings of Taylor et al. [39]. To draw a conclusion about the clinical impact of the suggested margins, we await the results of the ongoing multicenter RTOG-0418 on postoperative pelvic IMRT for the treatment of gynecologic malignancies. In the mean time, the issue of margins for pelvic IMRT should be viewed cautiously.

2.6 The Issue of Tumor Volume Regression and Organ Motion for IGRT and IGBT

The magnitude of tumor volume regression influences organ topography and, consequently the dosimetric parameters in pelvic IMRT [3, 5, 45–47]. Van de Bunt et al. [5] used MRI to investigate whether a replan of IMRT after delivering 30 Gy results in dose reduction to the bowel. DVH analysis demonstrated that bowel dose decreased significantly in those cervical cancer patients who had tumor regression >30 cm^3 on MRI. Dimopoulos et al. found that during EBRT ~50% of patients had a tumor volume reduction of >30 cm^3 on MRI, in ~40% a reduction of >40 cm^3 occurred and ~30% had a reduction of >50 cm^3. It was also shown that a significant tumor volume decrease (of some 25–30%) has to be expected during the last third of EBRT [3]. Lee et al. have studied changes in position and volume of the cervix during the course of both EBRT and high dose rate (HDR) brachytherapy using CT [20]. They estimated that 50% of tumor regression occurs after ~30 Gy and that it takes about 21 days to achieve it [20]. Available data advocate the adaptation of IMRT plan after the third week of treatment. The benefit of more frequent replanning for patients with rapid tumor response should be addressed in future treatment planning studies.

The impact of topographical organ changes between fractions on internal PTV margins for IMRT of cervical cancer was investigated by van de Bunt et al. by using weekly MR imaging [47]. The largest margins had to be applied in anterior and posterior directions (24 and 17 mm respectively), while margins of 12, 16, 11, and 8 mm were sufficient in right lateral, left lateral, superior, and inferior directions, respectively [47]. Taylor and Powell proposed an asymmetrical internal margin with CTV–PTV expansion of the uterus, cervix, and upper vagina of 15 mm anteriorly posteriorly, 15 mm superiorly inferiorly, and 7 mm laterally and expansion of the nodal regions and parametria by 7 mm in all directions [46]. Currently it seems that there is not enough evidence to suggest any widely applicable recommendations regarding the appropriate individualized internal PTV margin. Its adaptation shall be addressed with caution taking in consideration one's own experience.

During fractionated IGBT, the time-related topography between tumor/target and OAR is also taken into consideration (Fig. 2.3) [48, 49]. In a recent MRI-based study, measurements of volumes encompassing GTV at the time of brachytherapy (GTV_{BT}) and "grey zones" showed that tumor regression during HDR brachytherapy appeared to have some impact on organ topography as well [3]. The mean volume was reduced from 16 to 10 cm^3 between first and the second fractions with later minor reduction from 9 to 8 cm^3 between third and fourth fractions [3].

2.7 Conclusion

Both CT and MRI are widely used for image-guided radiotherapy of gynecological malignancies. CT is a standard imaging modality for treatment planning of EBRT, while MR represents the modality of choice for IGBT. MRI provides detailed information about

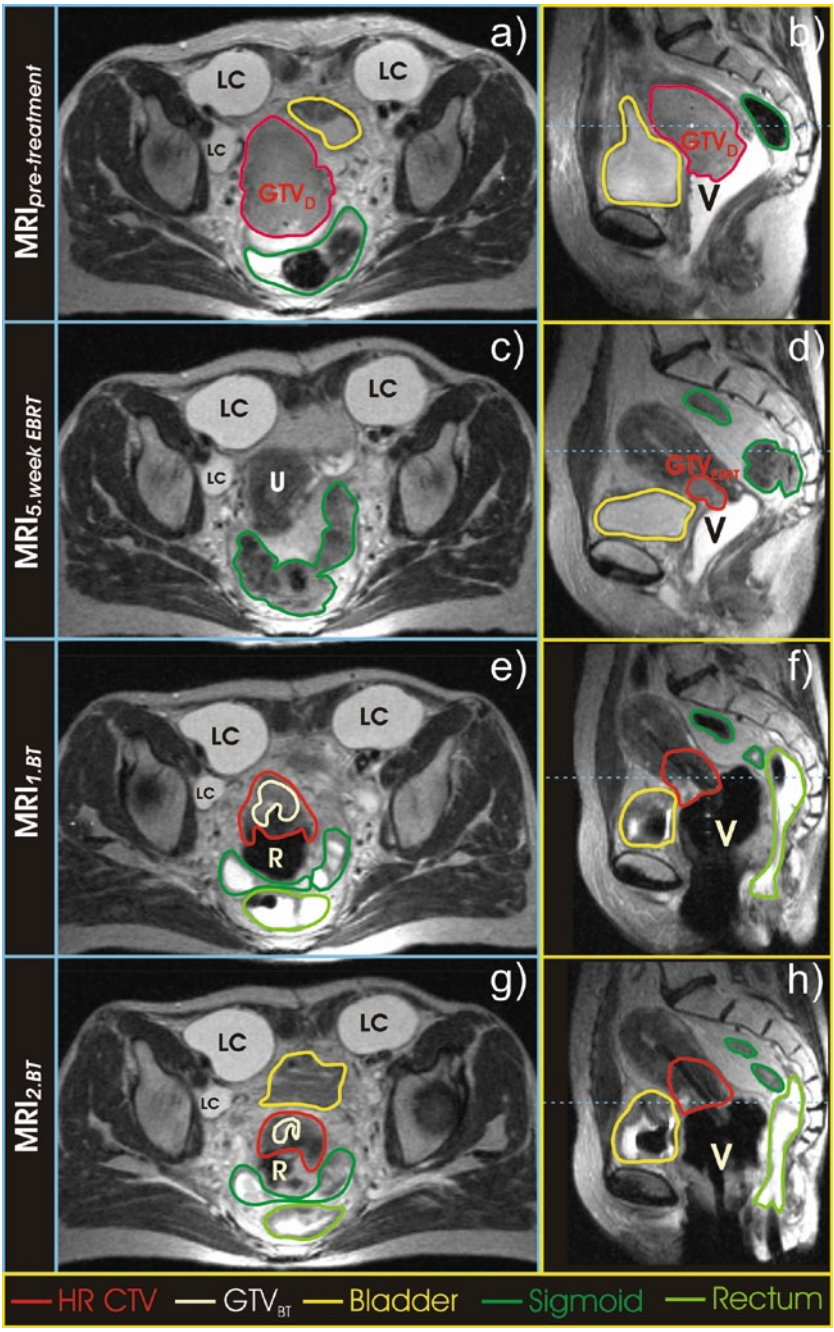
MRI pre-treatment
MRI 5.week EBRT
MRI 1.BT
MRI 2.BT
a)
b)
c)
d)
e)
f)
g)
h)
LC
GTV D
GTV EBRT
U
R
V
HR CTV
GTV BT
Bladder
Sigmoid
Rectum

Fig. 2.3 MRI scans of a patient with FIGO IIB cervical cancer at different time points of definitive radiochemotherapy. At diagnosis, a bulky tumor of cervix with proximal infiltration of both parametria is visible (GTV_D) (**a**, **b**). Significant tumor regression occurred during external beam radiotherapy (EBRT) and at the fifth week of treatment only small residual tumor of the anterior cervical lip is present (**d**). The axial scan at the fifth week (**c**) is taken at the same level, according to bony landmarks, as the pretreatment scan (**a**). It reveals normal uterine corpus and no evidence of tumor (**c**, **d**). At time of first (**e**, **f**) and second (**g**, **h**) BT further reduction of tumor is seen. *Dotted blue line* on sagittal images represents the level at which the correspondent axial scan was obtained (LC, lymphocyst after laparoscopic lymph node staging; GTV_D, gross tumor volume at diagnosis; V, vagina contrasted with ultrasound gel (**b, d**) or with packing impregnated with gadolinium (**f, h**); U, uterine corpus; R, ring)

tumor extension and enables accurate monitoring of tumor regression and organ movement during the entire course of IGRT and IGBT. Less precise information about tumor extension, tumor regression, and internal changes of organ and tumor topography can be obtained with CT. CTV margins for successful coverage of relevant lymph node regions derived from CT and MRI are comparable. The use of repetitive sectional imaging with treatment plan adaptation leads to reduction of the dose to the bowel during IGRT. Characteristics of tumor/target at diagnosis and at different time points of EBRT, which are essential for successful IGBT, are provided with higher accuracy by MRI.

Finally, it has to be stressed that IGRT has a potential not only to apply higher doses and to reduce margins around the tumor, but also to assure that interfraction variation in organ motion and patient setup are taken into account. Reduction of radiotherapy-related morbidity, improvement of locoregional control, and quality of life might be potential benefits of using repetitive imaging for IGRT. Those endpoints should be evaluated in future prospective randomized trials.

References

1. Tanyi JA, Fuss MH. Volumetric image-guidance: does routine usage prompt adaptive re-planning? An institutional review. Acta Oncol. 2008;47:1444–53.
2. Verellen D, De RM, Tournel K, et al. An overview of volumetric imaging technologies and their quality assurance for IGRT. Acta Oncol. 2008;47:1271–8.
3. Dimopoulos J, Schirl G, Baldinger A, Helbich T, Pötter R. MRI Assessment of Cervical Cancer for Adaptive Radiotherapy. Strahlenther Onkol. 2009;185:282–7.
4. Dimopoulos JC, Schard G, Berger D, et al. Systematic evaluation of MRI findings in different stages of treatment of cervical cancer: potential of MRI on delineation of target, pathoanatomic structures, and organs at risk. Int J Radiat Oncol Biol Phys. 2006;64:1380–8.
5. van de Bunt L, van der Heide UA, Ketelaars M, de Kort GA, Jurgenliemk-Schulz IM. Conventional, conformal, and intensity-modulated radiation therapy treatment planning of external beam radiotherapy for cervical cancer: the impact of tumor regression. Int J Radiat Oncol Biol Phys. 2006;64:189–96.
6. Chen Z, Ma CM, Paskalev K, et al. Investigation of MR image distortion for radiotherapy treatment planning of prostate cancer. Phys Med Biol. 2006;51:1393–403.

7. Khoo VS, Joon DL. New developments in MRI for target volume delineation in radiotherapy. Br J Radiol. 2006;79 Spec No 1:S2–15.
8. Kessler ML. Image registration and data fusion in radiation therapy. Br J Radiol. 2006;79 Spec No 1:S99–108.
9. Veninga T, Huisman H, van der Maazen RW, Huizenga H. Clinical validation of the normalized mutual information method for registration of CT and MR images in radiotherapy of brain tumors. J Appl Clin Med Phys. 2004;5:66–79.
10. Doran SJ, Charles-Edwards L, Reinsberg SA, Leach MO. A complete distortion correction for MR images: I. Gradient warp correction. Phys Med Biol. 2005;50:1343–61.
11. Fransson A, Andreo P, Potter R. Aspects of MR image distortions in radiotherapy treatment planning. Strahlenther Onkol. 2001;177:59–73.
12. Reinsberg SA, Doran SJ, Charles-Edwards EM, Leach MO. A complete distortion correction for MR images: II. Rectification of static-field inhomogeneities by similarity-based profile mapping. Phys Med Biol. 2005;50:2651–61.
13. Tanner SF, Finnigan DJ, Khoo VS, Mayles P, Dearnaley DP, Leach MO. Radiotherapy planning of the pelvis using distortion corrected MR images: the removal of system distortions. Phys Med Biol. 2000;45:2117–32.
14. Payne GS, Leach MO. Applications of magnetic resonance spectroscopy in radiotherapy treatment planning. Br J Radiol. 2006;79 Spec No 1:S16–26.
15. Norris DG. High field human imaging. J Magn Reson Imaging. 2003;18:519–29.
16. Viswanathan AN, Dimopoulos J, Kirisits C, Berger D, Potter R. Computed tomography versus magnetic resonance imaging-based contouring in cervical cancer brachytherapy: results of a prospective trial and preliminary guidelines for standardized contours. Int J Radiat Oncol Biol Phys. 2007;68:491–8.
17. Petric P, Dimopoulos J, Kirisits C, Berger D, Hudej R, Potter R. Inter- and intraobserver variation in HR CTV contouring: intercomparison of transverse and paratransverse image orientation in 3D-MRI assisted cervix cancer brachytherapy. Radiother Oncol. 2008;89:164–71.
18. Potter R. Modern imaging in Brachytherapy. In: Gerbaulet A, Potter R, Mazeron JJ, Meertens H, Van LE, editors. The GEC ESTRO Handbook of Brachytherapy. Brussels: European Society for Therapeutic Radiology and Oncology; 2002. p. 123–51.
19. Beadle BM, Jhingran A, Salehpour M, Sam M, Iyer RB, Eifel PJ. Cervix regression and motion during the course of external beam chemoradiation for cervical cancer. Int J Radiat Oncol Biol Phys. 2009;73:235–41.
20. Lee CM, Shrieve DC, Gaffney DK. Rapid involution and mobility of carcinoma of the cervix. Int J Radiat Oncol Biol Phys. 2004;58:625–30.
21. Potter R, Haie-Meder C, Van LE, et al. Recommendations from gynecological (GYN) GEC ESTRO working group (II): concepts and terms in 3D image-based treatment planning in cervix cancer brachytherapy-3D dose volume parameters and aspects of 3D image-based anatomy, radiation physics, radiobiology. Radiother Oncol. 2006;78:67–77.
22. Saarnak AE, Boersma M, van Bunningen BN, Wolterink R, Steggerda MJ. Inter-observer variation in delineation of bladder and rectum contours for brachytherapy of cervical cancer. Radiother Oncol. 2000;56:37–42.
23. Foshager MC, Walsh JW. CT anatomy of the female pelvis: a second look. Radiographics. 1994;14:51–64.
24. Vick CW, Walsh JW, Wheelock JB, Brewer WH. CT of the normal and abnormal parametria in cervical cancer. AJR Am J Roentgenol. 1984;143:597–603.
25. Walsh JW, Goplerud DR. Prospective comparison between clinical and CT staging in primary cervical carcinoma. AJR Am J Roentgenol. 1981;137:997–1003.
26. Hricak H, Lacey CG, Sandles LG, Chang YC, Winkler ML, Stern JL. Invasive cervical carcinoma: comparison of MR imaging and surgical findings. Radiology. 1988;166:623–31.

27. Hatano K, Sekiya Y, Araki H, et al. Evaluation of the therapeutic effect of radiotherapy on cervical cancer using magnetic resonance imaging. Int J Radiat Oncol Biol Phys. 1999;45: 639–44.
28. Mayr NA, Magnotta VA, Ehrhardt JC, et al. Usefulness of tumor volumetry by magnetic resonance imaging in assessing response to radiation therapy in carcinoma of the uterine cervix. Int J Radiat Oncol Biol Phys. 1996;35:915–24.
29. Mayr NA, Taoka T, Yuh WT, et al. Method and timing of tumor volume measurement for outcome prediction in cervical cancer using magnetic resonance imaging. Int J Radiat Oncol Biol Phys. 2002;52:14–22.
30. Kim SH, Choi BI, Lee HP, et al. Uterine cervical carcinoma: comparison of CT and MR findings. Radiology. 1990;175:45–51.
31. Kim SH, Choi BI, Han JK, et al. Preoperative staging of uterine cervical carcinoma: comparison of CT and MRI in 99 patients. J Comput Assist Tomogr. 1993;17:633–40.
32. Yang WT, Lam WW, Yu MY, Cheung TH, Metreweli C. Comparison of dynamic helical CT and dynamic MR imaging in the evaluation of pelvic lymph nodes in cervical carcinoma. AJR Am J Roentgenol. 2000;175:759–66.
33. Manfredi R, Mirk P, Maresca G, et al. Local-regional staging of endometrial carcinoma: role of MR imaging in surgical planning. Radiology. 2004;231:372–8.
34. Rockall AG, Sohaib SA, Harisinghani MG, et al. Diagnostic performance of nanoparticle-enhanced magnetic resonance imaging in the diagnosis of lymph node metastases in patients with endometrial and cervical cancer. J Clin Oncol. 2005;23:2813–21.
35. Scheidler J, Heuck AF. Imaging of cancer of the cervix. Radiol Clin North Am. 2002;40: 577–90, vii.
36. Kitajima K, Murakami K, Yamasaki E, et al. Accuracy of 18F-FDG PET/CT in detecting pelvic and paraaortic lymph node metastasis in patients with endometrial cancer. AJR Am J Roentgenol. 2008;190:1652–8.
37. Loft A, Berthelsen AK, Roed H, et al. The diagnostic value of PET/CT scanning in patients with cervical cancer: a prospective study. Gynecol Oncol. 2007;106:29–34.
38. Park JY, Kim EN, Kim DY, et al. Comparison of the validity of magnetic resonance imaging and positron emission tomography/computed tomography in the preoperative evaluation of patients with uterine corpus cancer. Gynecol Oncol. 2008;108:486–92.
39. Small Jr W, Mell LK, Anderson P, et al. Consensus guidelines for delineation of clinical target volume for intensity-modulated pelvic radiotherapy in postoperative treatment of endometrial and cervical cancer. Int J Radiat Oncol Biol Phys. 2008;71:428–34.
40. Taylor A, Rockall AG, Powell ME. An atlas of the pelvic lymph node regions to aid radiotherapy target volume definition. Clin Oncol (R Coll Radiol). 2007;19:542–50.
41. Chao KS, Lin M. Lymphangiogram-assisted lymph node target delineation for patients with gynecologic malignancies. Int J Radiat Oncol Biol Phys. 2002;54:1147–52.
42. Dinniwell R, Chan P, Czarnota G, et al. Pelvic lymph node topography for radiotherapy treatment planning from ferumoxtran-10 contrast-enhanced magnetic resonance imaging. Int J Radiat Oncol Biol Phys. 2009 Jul 1;74:844–51.
43. Taylor A, Rockall AG, Reznek RH, Powell ME. Mapping pelvic lymph nodes: guidelines for delineation in intensity-modulated radiotherapy. Int J Radiat Oncol Biol Phys. 2005;63: 1604–12.
44. Vilarino-Varela MJ, Taylor A, Rockall AG, Reznek RH, Powell ME. A verification study of proposed pelvic lymph node localisation guidelines using nanoparticle-enhanced magnetic resonance imaging. Radiother Oncol. 2008;89:192–6.
45. Lim K, Chan P, Dinniwell R, et al. Cervical cancer regression measured using weekly magnetic resonance imaging during fractionated radiotherapy: radiobiologic modeling and correlation with tumor hypoxia. Int J Radiat Oncol Biol Phys. 2008;70:126–33.

46. Taylor A, Powell ME. An assessment of interfractional uterine and cervical motion: implications for radiotherapy target volume definition in gynecological cancer. Radiother Oncol. 2008;88:250–7.
47. van de Bunt L, Jurgenliemk-Schulz IM, de Kort GA, Roesink JM, Tersteeg RJ, van der Heide UA. Motion and deformation of the target volumes during IMRT for cervical cancer: what margins do we need? Radiother Oncol. 2008;88:233–40.
48. Haie-Meder C, Potter R, Van LE, et al. Recommendations from Gynecological (GYN) GEC-ESTRO Working Group (I): concepts and terms in 3D image based 3D treatment planning in cervix cancer brachytherapy with emphasis on MRI assessment of GTV and CTV. Radiother Oncol. 2005;74:235–45.
49. Kirisits C, Potter R, Lang S, Dimopoulos J, Wachter-Gerstner N, Georg D. Dose and volume parameters for MRI-based treatment planning in intracavitary brachytherapy for cervical cancer. Int J Radiat Oncol Biol Phys. 2005;62:901–11.

http://www.springer.com/978-3-540-68954-6

Gynecologic Radiation Therapy
Novel Approaches to Image-Guidance and Management
Viswanathan, A.N.; Kirisits, C.; Erickson, B.E.; Pötter, R. (Eds.)
2011, IX, 308 p., Hardcover
ISBN: 978-3-540-68954-6